Epilepsia, 53(1):25–34, 2012
doi: 10.1111/j.1528-1167.2011.03333.x

FULL-LENGTH ORIGINAL RESEARCH

Gray matter loss correlates with mesial temporal lobe neuronal hyperexcitability inside the human seizure-onset zone

***Richard J. Staba, †Arne D. Ekstrom, ‡Nanthia A. Suthana, §¶Alison Burggren, ‡Itzhak Fried, *¶#**Jerome Engel Jr, and §¶Susan Y. Bookheimer**

***Department of Neurology, David Geffen School of Medicine, University of California, Los Angeles, California, U.S.A.; †Center for Neuroscience, Department of Psychology, University of California, Davis, California, U.S.A.; ‡Department of Neurosurgery, David Geffen School of Medicine, University of California, Los Angeles, California, U.S.A.; §Center for Cognitive Neurosciences, Semel Institute, University of California, Los Angeles, California, U.S.A.; ¶Department of Psychiatry and Biobehavioral Sciences, Semel Institute, University of California, Los Angeles, California, U.S.A.; #Department of Neurobiology, David Geffen School of Medicine, University of California, Los Angeles, California, U.S.A.; and **Brain Research Institute, David Geffen School of Medicine, University of California, Los Angeles, California, U.S.A.**

Summary

Purpose: Patient studies have not provided consistent evidence for interictal neuronal hyperexcitability inside the seizure-onset zone (SOZ). We hypothesized that gray matter (GM) loss could have important effects on neuronal firing, and quantifying these effects would reveal significant differences in neuronal firing inside versus outside the SOZ.

Methods: Magnetic resonance imaging (MRI) and computational unfolding of mesial temporal lobe (MTL) subregions was used to construct anatomic maps to compute GM loss in presurgical patients with medically intractable focal seizures in relation to controls. In patients, these same maps were used to locate the position of microelectrodes that recorded interictal neuronal activity. Single neuron firing and burst rates were evaluated in relation to GM loss and MTL subregions inside and outside the SOZ.

Key Findings: MTL GM thickness was reduced inside and outside the SOZ in patients with respect to controls, yet GM loss was associated more strongly with firing and burst rates in several MTL subregions inside the SOZ. Adjusting single neuron firing and burst rates for the effects of GM loss revealed significantly higher firing rates in the subregion consisting of dentate gyrus and CA2 and CA3 (CA23DG), as well as CA1 and entorhinal cortex (EC) inside versus outside the SOZ where normalized MRI GM loss was ≥1.40 mm. Firing rates were higher in subicular cortex inside the SOZ at GM loss ≥1.97 mm, whereas burst rates were higher in CA23DG, CA1, and EC inside than outside the SOZ at similar levels of GM loss.

Significance: The correlation between GM loss and increased firing and burst rates suggests GM structural alterations in MTL subregions are associated with interictal neuronal hyperexcitability inside the SOZ. Significant differences in firing rates and bursting in areas with GM loss inside compared to outside the SOZ indicate that synaptic reorganization following cell loss could be associated with varying degrees of epileptogenicity in patients with intractable focal seizures.

KEY WORDS: Epilepsy, Atrophy, Hippocampus, Magnetic resonance imaging, Microelectrode, Single neuron.

Experimental models of focal seizures show that neuronal burst firing occurs regularly within the interictal electroencephalographic spike focus (Matsumoto & Marsan, 1964; Sherwin, 1970; Reid & Sypert, 1980), supporting the concept that abnormal excitability, for example, higher firing rates, bursting, or both, contributes to the generation of epileptiform discharges. It would be reasonable to expect then that in patients with pharmacoresistant focal seizures, the seizure-onset zone (SOZ) would also contain a significant number of abnormally firing neurons. Interictal single neuron studies, however, have not provided evidence wholly consistent with results from experimental models (Isokawa-Akesson et al., 1989; Colder et al., 1996a,b; Staba et al., 2002b; Viskontas et al., 2007). Furthermore, in vitro studies have also had difficultly detecting abnormal firing because resected epileptogenic tissue might not maintain spontaneous synaptic activity (Schwartzkroin et al., 1983), but electrical stimulation in dentate gyrus shows abnormal evoked responses correlate with higher levels of

Accepted October 6, 2011; Early View publication November 29, 2011.
Address correspondence to Richard J. Staba, Reed Neurological Research Center, Westwood Plaza, Room 2155, 710 Los Angeles, CA 90095, U.S.A. E-mail: rstaba@mednet.ucla.edu

Wiley Periodicals, Inc.

axon sprouting (Masukawa et al., 1992). These latter data suggest that hyperexcitability might also be associated with levels of neuron loss, which was not considered in the patient studies cited above and could explain differences in results from these studies, as well as provide new information on neuronal disturbances inside the SOZ.

In patients with poorly controlled focal seizures arising from the mesial temporal lobe (MTL), quantitative magnetic resonance imaging (MRI) studies can detect mesial temporal lobe (MTL) abnormalities ipsilateral and contralateral to the temporal (Hogan et al., 2004; Lin et al., 2007; Labate et al., 2008; McDonald et al., 2008; Ogren et al., 2009a) or extratemporal lobe SOZ (Scott et al., 2003; Briellmann et al., 2004). In some of these studies using advance neuroimaging techniques, intracranial depth electrodes with microelectrodes can be registered with MRI to investigate electrophysiologic disturbances in relation to structural damage (Ekstrom et al., 2008; Ogren et al., 2009a,b). In the present study, high-resolution MRI and computational unfolding of the MTL was used to construct gray matter (GM) thickness maps in presurgical patients and controls. In patients, these same anatomic maps were used to register the position of microelectrodes that recorded interictal single neuron activity to determine whether changes in GM thickness were associated with neuronal firing and burst rates, and if so, whether adjusting for the effects of GM loss would identify differences in MTL firing and burst rates inside compared to outside the SOZ.

Materials and Methods

Subjects

Subjects for this retrospective study were 10 consecutive patients (three female) with intractable focal seizures that began in temporal or extratemporal structures (Table 1), and 13 controls (three female) without epilepsy [patient vs. control, mean age ± standard deviation (SD) 36.3 ± 10.5 vs. 30.5 ± 10.4 years, $t = 1.3$, $p = 0.10$). Patients were candidates for epilepsy surgery, but required clinical depth electrode studies to locate brain areas where seizures began because results from noninvasive studies were not conclusive. In each patient, seven contact depth electrodes (AdTech Medical Instruments, Racine, WI, U.S.A.) were implanted bilaterally in temporal and frontal lobe areas, orthogonal to the lateral skull surface, to identify brain areas generating spontaneous seizure activity (Engel, 1996). All patients gave their informed consent to participate in this study, which was approved by the medical institutional review board in the UCLA Office for Protection of Research Subjects.

Microelectrode single neuron recordings

Inserted through the lumen of each depth electrode was a microelectrode that consisted of a linear array of nine, 40-μm diameter platinum-iridium microwires that extended ≤4 mm beyond the tip (impedance 100–300 kΩ at 1 kHz; 500 μm intertip spacing) (Fried et al., 1999). The ninth microwire in each bundle was uninsulated and was used as reference (impedance 1–3 kΩ at 1 kHz). Continuous wide bandwidth (0.001–6 kHz, 27.8 kHz sampling; 16-bit precision, Neuralynx, Inc., Bozeman, MT, U.S.A.) depth electroencephalography (EEG) was recorded from 64 microwires simultaneously 72 h after surgery between 2200 and 0700 h while patients were maintained on presurgical levels of antiepileptic drugs (AEDs) and at least 12 h before or after a spontaneous seizure. For each patient, recordings between 60 and 120 min in duration were analyzed. Extracellular action potentials (“spikes”) were detected from bandpass filtered (0.3–3 kHz, 4th order elliptical filter) high-frequency EEG and 2.3 ms (64 data points) surrounding the

Table 1. Patient clinical data

Pt	Age/sex/handedness	Duration of epilepsy[a]	Seizure onset	MRI	Surgery		Pathology
					Resection	Outcome[b]	
1	38/M/R	30	R Am, AH, EC	R AH atrophy	R AMTL	I (32)	HS
2	20/M/R	7	R Am, AH; L Par	R AH atrophy; L Par schizencephaly	–	–	
3	54/M/L	52	R ATL; L ATL	L Temp atrophy	–	–	
4	31/M/R	24	R AH, PHG	Negative	[c]	–	
5	43/M/R	27	R Am, AH, EC	Negative	R AMTL	I (22)	Gliosis
6	27/M/R	18	L ATL	L ATL atrophy	L ATL	I (23)	Mild CD
7	42/F/R	15	R OF, pSMA	R OF, pSMA CD	R F lesionectomy	I (19)	Palmini type IIB
8	46/M/R	29	R OF; L OF	Negative	–	–	
9	25/F/R	15	R AH; L AH, EC	Negative	–	–	
10	37/F/R	35	R Am, AH, EC	R Am, AH atrophy	R AMTL	I (5)	Mild HS

L, left; R, right; AH, anterior hippocampus; Am, amygdala; AMTL, anterior mesial temporal lobe resection; ATL, anterior temporal lobe; CD, cortical dysplasia; EC, entorhinal cortex; HS, hippocampal sclerosis; OF, orbital frontal cortex; Par, parietal lobe; PHG, parahippocampal gyrus; pSMA, presupplementary motor area.

[a]Duration of epilepsy expressed in years at time of depth electrode evaluation.

[b]Postsurgical outcome class based on Engel classification I–IV (Engel 1993). Number in parentheses is follow-up in months.

[c]Patient offered surgery, but declined citing reduction in seizures after depth electrode evaluation.

minimum amplitude of the central trough of each spike waveform was extracted (Fig. S1). An automated spike sorting algorithm called Osort was used to cluster spikes based on waveform similarities (Rutishauser et al., 2006). Each cluster was visually inspected and resorted manually if >2% of the total interspike intervals (ISIs) occurred between 0 and 2 ms, or if results from projection tests, which measured the extent of separation between two clusters, found >1% overlap between respective spike distributions. Clusters unsuccessfully sorted and/or containing a narrow peak in power at 60 Hz in the power spectral density histogram were excluded from further analysis. Overall, 88 ± 13% of all detected spikes were successfully sorted into individual clusters corresponding to putative single neurons.

MRI acquisition and analysis

Structural MRI analysis was similar to that in previous patient studies and summarized in Fig. 1 (Zeineh et al., 2001, 2003; Ekstrom et al., 2009b). For all patients a 3 Tesla T_2-weighted MRI (repetition time 5.2 s, echo time 105 ms, 19 contiguous slices, voxel size $0.4 \times 0.4 \times 3.0$ mm) of the MTL was obtained in the coronal plane perpendicular to the anterior-posterior axis (AP) of the hippocampus (Fig. 1A). GM was segmented by outlining white matter and cerebral spinal fluid (CSF) along the hippocampus proper and extending through the fusiform cortex (Fig. 1B,C). Coronal slices were mathematically interpolated by a factor of 7, which produced a final voxel size of $0.4 \times 0.4 \times 0.43$ mm, and then GM voxels were connected using the region-expansion algorithm MrGray that produced a 3D GM strip (Teo et al., 1997) (Fig. 1D). The 3D strip was computationally flattened into 2D using MRUNFOLD software (Fig. 1F) (Engel et al., 1997). Because distinct cytoarchitectural boundaries corresponding to MTL subregions could not be detected on MRI, a rules-based protocol combined with atlases of hippocampal structural anatomy (Mai et al., 1997; Duvernoy, 1998; Amaral, 1999) was used to manually draw margins that separated MTL subregions on three-dimensional (3D) hippocampal images (Fig. 1E). Due to the highly convoluted nature of dentate gyrus (DG) and hippocampal subfields CA2 and CA3, these areas were combined (CA23DG); CA23DG–CA1; CA1–subicular cortex (SUB); SUB–entorhinal cortex (EC); EC–perirhinal cortex (PRC); SUB–parahippocampal gyrus (PHG); and PHG–fusiform cortex (i.e., the collateral sulcus). We also demarcated the beginning of the hippocampal head and the EC-PRC-PHG boundary. Margins derived in 3D were then projected onto unfolded two-dimensional (2D) maps that outlined each MTL subregion (Fig. 1F).

GM thickness was measured by first extracting the middle layer in the 3D GM strip (e.g., Fig. 1D), which was equidistant from adjacent white matter and CSF, and then the distance value at each GM voxel in the middle layer was multiplied by two (Burggren et al., 2008). Mean GM thickness was computed for each MTL subregion by averaging thickness values from all GM voxels within the margins on the 2D maps (Fig. 1F). Individual MTL subregions were normalized by multiplying each subregion thickness by the grand mean total number of voxels from the right and left MTL and dividing by the total number of voxels in the corresponding MTL.

Localization of microelectrode arrays used the same techniques described in previous studies and in relation to anatomic maps, arrays typically encompassed an 8 mm^2 area with 1 mm in-plane accuracy (Ekstrom et al., 2008, 2009a,b). A three-way registration was carried out using preoperative 3 Tesla T_1- and T_2-weighted MRI and postimplantation computed tomography (CT) (1 s rotation, helical pitch 1.5, 1 mm slice collimation, 0.5 mm reconstruction interval delineated using axial slices) using IPLAN software (BRAINLAB Munich, Germany) (Gumprecht et al., 1999; Schlaier et al., 2004). CT images were manually reviewed in 3D for signal artifact corresponding to the microelectrode extending beyond the tip of each clinical depth electrode (Fig. 1G), and visually verified with microelectrode array trajectories on skull radiograph scans. Coordinates corresponding with marked microelectrode tips on CT were registered to locations on MRI. In all cases, the position of microelectrodes on 3D T_1-weighted MRI corresponded with those on 3D T_2-weighted MRI and 2D MTL map.

Data analysis

Brain areas of depth EEG seizure onset were identified by group consensus of neurologists at UCLA following review of multiple spontaneous, independent seizures. Using sites of seizure onset and early propagation based on results from previous work (Lieb et al., 1986), MTL where seizures began or appeared ≤5 s from sites of onset were labeled ''inside the SOZ,'' whereas the MTL where onsets did not occur or seizures appeared >5 s from sites of onset were labeled ''outside the SOZ.'' In patients with bilateral temporal lobe onsets (n = 2), left and right MTL were considered inside the SOZ, whereas in patients (n = 2) with extratemporal onsets and no appearance of seizures ≤5 s from the site of onset, left and right MTL were considered outside the SOZ.

Single neuron firing properties included mean firing rate (spikes/s), mean burst rate (bursts/min), and percentage of spikes in bursts. A rank surprise method was used to identify bursts defined as an episode of ≥n consecutive spikes with <i ISI that would be unexpected if the ISIs were randomly and independently drawn from the neuron's ISI distribution (Gourévitch & Eggermont, 2007). Burst parameters were $n \geq 3$ and i < duration in msec corresponding to the initial peak in each neuron's natural log-transformed ISI histogram (Selinger et al., 2007). Only bursts with a significant rank surprise statistic ($p < 0.01$) were used in measures of bursting.

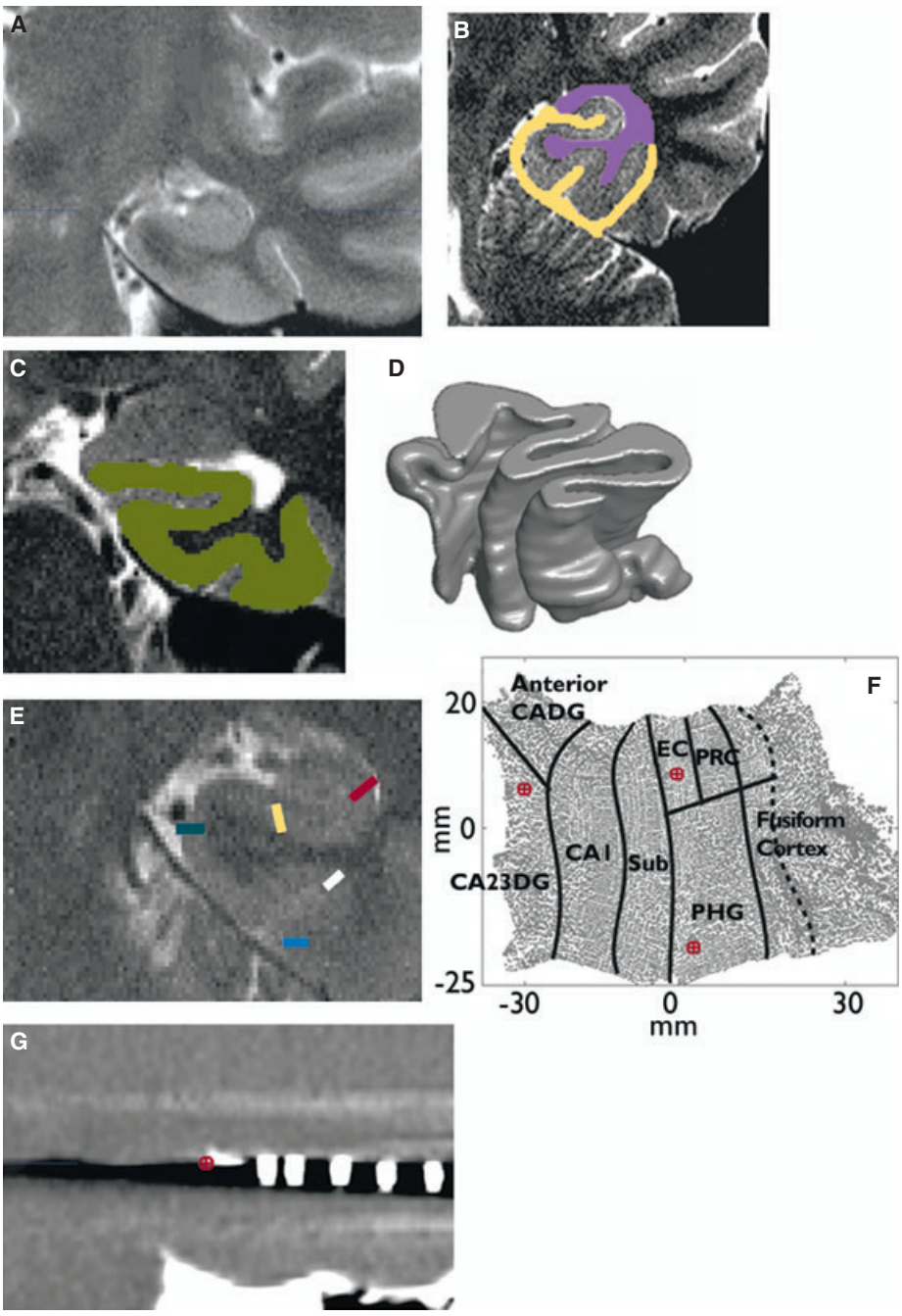

Figure 1.
MRI-based MTL GM thickness maps. Panels illustrate unfolding technique for left MTL viewed in coronal plane, but methods were carried out bilaterally in each patient's MRI. (**A**) 3 Tesla T_2-weighted MRI was acquired perpendicular to the anterior-posterior axis of the hippocampus. (**B** and **C**) MTL GM (green in **C**) was segmented manually by excluding CSF (yellow) and white matter (purple). (**D**) MTL GM strip was mathematically up-sampled, expanded, and smoothed to generate 3D GM ribbon. (**E**) A rules-based protocol and atlases of histologic and structural hippocampal anatomy were used to draw MTL subregion margins. The colored lines denote margins between CA23DG and CA1 (red), CA1 and SUB (yellow), SUB and EC (blue), EC and PRC (white), and PRC and FUS (light blue). (**F**) Computationally unfolded 2D map that contains margins corresponding to MTL subregions. (**G**) Example of postimplantation CT used to determine position of microelectrodes on MRI. White thick bands correspond with signal artifact from macroelectrodes, whereas the elongated white artifact corresponds with microelectrode array (tip indicated by red circle). Coordinates corresponding to each marked microelectrode identified their position on a 2D anatomic maps (c.f. panel **F**).

Statistical analysis was carried out using SPSS Statistics software (IBM Corp., Somers, NY, U.S.A.). Analysis of variance was used to compare normalized GM thickness between subject groups (patient vs. control) and epileptogenicity (inside vs. outside the SOZ), with MTL subregion as the within-group repeated measure. An analysis of covariance (ANCOVA) model was used to compare firing and burst rates in relation to epileptogenicity and MTL subregion, using subregion GM loss (or gain) as a covariate computed as the difference in normalized mean GM thickness between patient and matched controls. In the ANCOVA, standardized values of rates and GM loss were used, and regression analysis was used to evaluate significant interactions with GM loss. Each subgroup in the interaction with GM loss was evaluated independently, and a systematic comparison was carried out to determine whether subgroup slopes were statistically different. Subgroups that had the same slope were combined to reduce the number of independent variables in the model, and then a separate analysis was carried out to determine whether the pooled subgroup slopes were significantly different than zero and from one another. ANCOVA assumes homogeneity of regression (i.e., equal slopes between GM loss and rates), and for post hoc analysis with unequal slopes, rates were adjusted using the following equation and evaluated at specific levels of GM thickness: $Y_{adj} = Y_{unadj} - B \times (X_{group} - X_{grand})$, where Y_{adj} and Y_{unadj} = adjusted and unadjusted mean rate, respectively, B = regression coefficient, and X_{group} and X_{grand} = group and grand mean of subregion GM thickness, respectively.

Results

MTL GM thickness

The MRI segmentation techniques illustrated in Fig. 1 were used to measure GM thickness in MTL subregions bilaterally of 10 patients with epilepsy and 13 age- and gender-matched controls. Overall, compared to controls, there was a significant reduction in mean normalized MTL GM thickness in patients inside and outside the SOZ ($F_{1,42} = 7.33$ $p = 0.009$; Fig. 2A). Moreover, significant differences were found between controls and subregions ($F_{6,252} = 5.22$, $p < 0.0001$), and Fig. 2B shows GM thickness for each MTL subregion in patients with respect to controls. Post hoc analyses found significantly reduced GM thickness in a combined area consisting of hippocampal CA2, CA3 and dentate gyrus labeled "CA23DG," subicular cortex (SUB), entorhinal cortex (EC), and fusiform gyrus (FUS). Differences in GM thickness between patients and controls in CA1, perirhinal cortex (PRC), and parahippocampal gyrus (PHG) were not statistically significant.

Single neuron firing rates

A total of 43 microelectrode arrays representing 344 active microwires were positioned bilaterally in most MTL subregions, except PRC or FUS, which were not sampled with microwires in this consecutive series of patients. Of the total microwires, 168 recorded extracellular spikes that were extracted and separated into 387 single neuron spike trains (Fig. S1). Table 2 shows the number of single

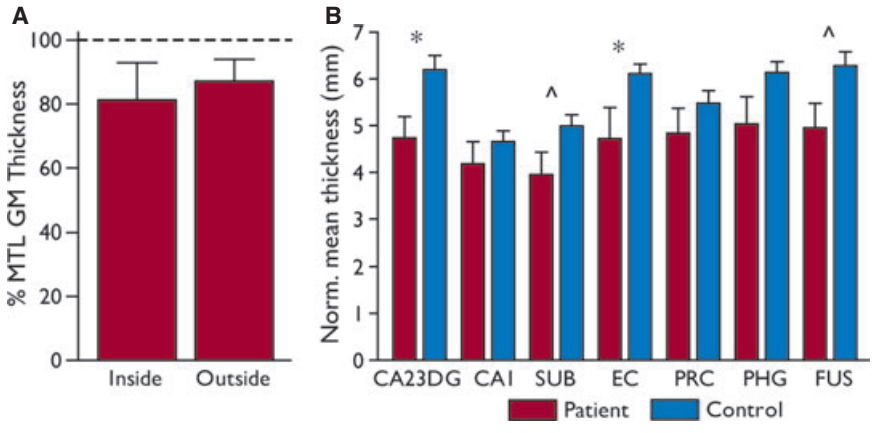

Figure 2.
MTL GM thickness in patients. (**A**) Mean MTL GM thickness in patients was significantly reduced compared to controls ($p = 0.0009$). MTL GM thickness inside and outside the SOZ in patients is expressed as percentage of controls set at 100%. All values in **A** and **B** reflect normalized GM thickness values. (**B**) Post hoc analysis showed that compared to controls, patients had the largest reductions in thickness in CA23DG (*$p = 0.001$), subicular (SUB; ^$p = 0.003$), and entorhinal cortex (EC), and fusiform gyrus (FUS) compared to controls. Differences in GM thickness were not significant in CA1 ($p = 0.31$), perirhinal cortex (PRC; $p = 0.29$), and parahippocampal gyrus (PHG; $p = 0.03$).

Table 2. Number of MTL single neurons inside and outside the SOZ

	CA23DG	CA1	SUB	EC	PHG	Total
Inside SOZ	75	21	9	36	57	198
Outside SOZ	53	22	45	48	21	189

neurons in relation to SOZ and subregion used in subsequent analyses.

An analysis of firing rates found no main effect of epileptogenicity ($F_{1,369} = 0.52$, $p = 0.47$), but there was a significant interaction between epileptogenicity and subregion ($F_{4,369} = 3.70$, $p = 0.006$; Table S1). Furthermore, there was a significant three-way interaction in epileptogenicity, subregion, and subregion GM loss computed as the difference in mean GM thickness between patient and matched controls ($F_{4,369} = 2.88$, $p = 0.02$). The latter interaction indicated the effects of GM loss on firing rates were different across subregions inside and outside the SOZ. As described in the Materials and Methods (in Data analysis section), regression analysis was used to evaluate each subgroup in the interaction independently, and if subgroups had equal slopes, then these were combined. Results of this analysis found GM loss was associated with higher firing rates in CA23DG, CA1, and EC inside the SOZ (Fig. 3A). By contrast, there was a smaller effect of GM loss on firing rates in SUB and PHG within the SOZ, as well as in all subregions outside the SOZ (Fig. 3B). A separate regression analysis revealed GM loss was associated with higher firing rates inside the SOZ ($F_{1,84} = 4.30$, $p = 0.04$), but not outside the SOZ ($F_{1,69} = 1.18$, $p = 0.28$), in the four patients who did not have gross MTL abnormalities on MRI, which was similar to the effect found in the overall group analysis. Analysis of fitted regression lines in Fig. 3A,B showed each slope was significantly different than zero, and the slopes were significantly different for each other ($F_{1,354} = 6.75$, $p = 0.01$).

Because regression analysis found unequal slopes, firing rates were adjusted for the different effects of GM loss, and the evaluation of rates in relation to epileptogenicity and subregion was carried out at different levels of GM loss. At normalized GM loss ≥1.40 mm, corresponding to the 50th percentile of GM loss in patients with respect to controls, firing rates were significantly higher in CA23DG, CA1, and EC inside the SOZ compared to homotopic subregions outside the SOZ (Fig. 3C). At levels of GM loss ≥1.97 mm, equivalent to the 25th percentile, significantly higher firing rates were found in SUB inside versus outside the SOZ. In contrast, at GM loss ≤0.26 mm corresponding to the 75th percentile (i.e., little or no GM loss in patients), firing rates in PHG inside the SOZ were lower than rates outside the SOZ.

Burst firing

MTL single neurons had irregular firing patterns that consisted of short episodes of a high rate of firing that were followed by longer periods of low or no firing (Fig. 4A). Coefficient of variation (CV) values were significantly greater than one (one sample *t*-test, $t = 7.02$, $p < 0.0001$), which was consistent with the occurrence of bursting (Wilbur & Rinzel, 1983). No difference was found in mean CV values inside versus outside the SOZ (1.37 ± 0.08 vs. 1.34 ± 0.07; $p = 0.32$), across subregions, or the interaction between epileptogenicity and subregion. The algorithm used to detect extracellular bursts included an ISI threshold

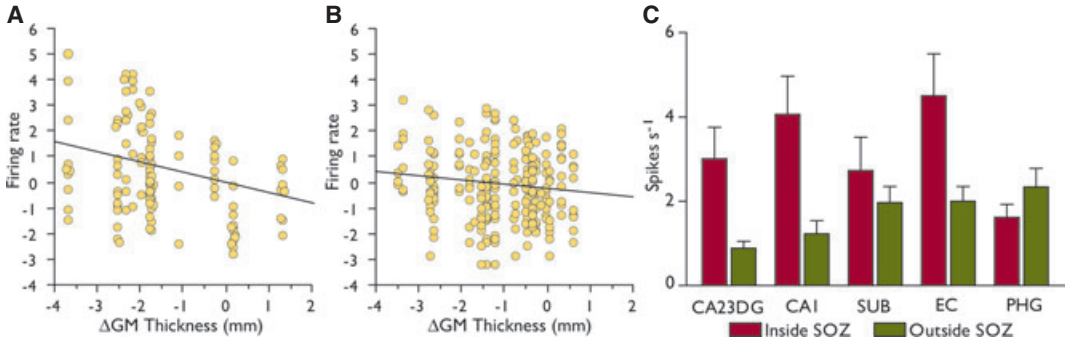

Figure 3.
Change (Δ) in normalized GM thickness in relation to MTL single neuron firing rates. (**A** and **B**) Results of regression analysis (denoted by solid lines) found a larger effect of GM thickness on rates in CA23DG, CA1, and EC inside the SOZ (**A**; slope vs. 0: $t = -4.30$, $p < 0.0001$; $r = 0.36$) than SUB and PHG inside the SOZ and MTL subregions outside the SOZ (**B**; slope vs. 0: $t = -2.17$, $p = 0.03$; $r = 0.14$). ΔGM thickness measured as patient minus matched control, and values <0 indicate GM loss, whereas values >0 indicate GM gain in patients. Firing rates are expressed as standardized values to more clearly show variability among rates. (**C**) Mean firing rates adjusted for ΔGM thickness in subregions with respect to SOZ. Significant differences were found in CA23DG ($p \leq 0.01$), CA1 ($p \leq 0.02$), and EC ($p \leq 0.01$) at ΔGM thickness of ≤−1.40 mm, SUB ($p \leq 0.01$) at ΔGM thickness of ≤−1.97 mm, and PHG ($p \leq 0.02$) at ΔGM thickness of ≥−0.26 mm.

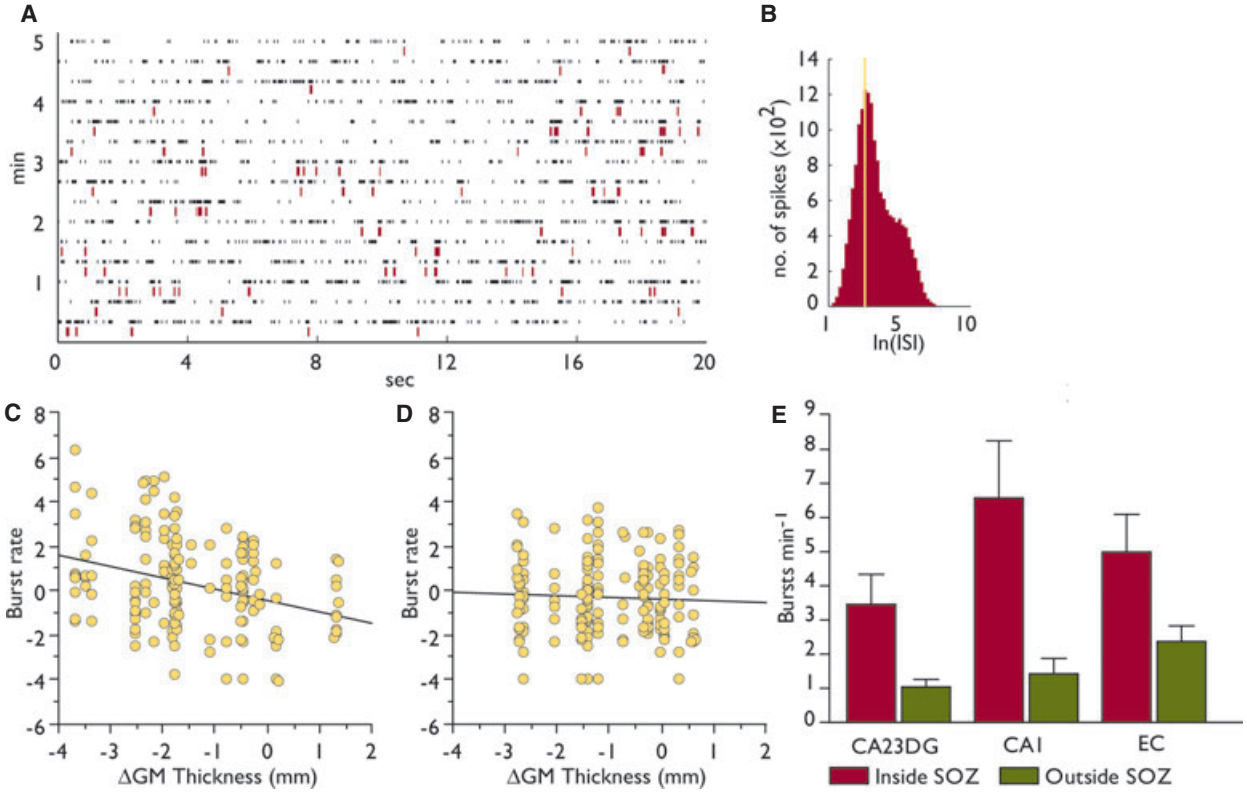

Figure 4.

Burst firing patterns. (**A**) Raster plot illustrating firing pattern from a single neuron in consecutive 20 s sweeps (x-axis) over a 5 min episode (*y*-axis). Black tick marks denote spike firing and red ticks directly below indicate bursts of spikes. (**B**) Natural log-transformed interspike interval (ISI) histogram on the right side from same neuron in raster shows a central peak in ISI distribution at 20 ms, which was used as the intraburst ISI threshold in the detection of bursts for this neuron. (**C** and **D**) Scatter plots of Δ in normalized GM thickness versus MTL single neuron burst rates. Results of regression analysis (indicated by solid lines) found a larger effect ΔGM thickness on burst rates inside the SOZ (**C**; regression line, r = 0.32) compared to burst rates outside the SOZ (**D**; regression line, r = 0.04). (**E**) Significant differences in mean burst rates adjusted for ΔGM thickness in CA23DG ($p \leq 0.03$) at ΔGM thickness of ≤−1.40 mm, and CA1 ($p \leq 0.05$) and EC ($p \leq 0.01$) at ΔGM thickness of ≤−1.97 mm.

derived from each neuron's ISI distribution (Fig. 4B; see Materials and Methods). Overall, median thresholds were 36 and 54 msec to extract bursts within and outside the SOZ, respectively, and no difference was found in distribution of ISI thresholds with respect to epileptogenicity (Mann–Whitney, $p = 0.35$). Eighty-seven percent of all neurons discharged spikes within bursts, and there was no difference in the percentage of spikes in bursts to total spikes with respect to epileptogenicity (inside SOZ, 9.10 ± 0.42%; outside SOZ, 9.45 ± 0.41%; $F_{1,369} = 0.20$, $p = 0.65$), across subregions, or with GM loss.

No difference was found in burst rates inside versus outside the SOZ ($F_{1,369} = 0.40$, $p = 0.53$), but there was a significant interaction between epileptogenicity and subregion ($F_{4,369} = 2.70$, $p = 0.03$), as well as a three-way interaction of epileptogenicity, subregion, and GM loss on burst rates ($F_{4,369} = 2.99$, $p = 0.02$). The same approach used for firing rates was used to evaluate the interaction with GM loss on burst rates. The scatter plot in Fig. 4C summarizes the results of the regression analysis that found GM loss was associated with higher burst rates in all subregions inside the SOZ. The slope quantifying this effect was significantly different than zero ($t = -4.59$, $p < 0.0001$), and different from the slope of the second regression line between GM loss and burst rates in subregions outside the SOZ shown in Fig. 4D ($F_{1,354} = 6.71$, $p = 0.01$). The effect of GM loss on burst rates outside the SOZ was much smaller, and the slope quantifying this effect was not different than zero ($t = -0.56$, $p = 0.58$). Post hoc analyses comparing burst rates in relation to epileptogenicity and subregion revealed that at GM loss ≥1.40 mm, burst rates were higher in CA23DG inside than outside the SOZ (Fig. 4E). At GM loss ≥1.97 mm, burst rates were significantly greater in CA1 and EC inside compared to outside the SOZ. No difference in adjusted mean burst rates was observed at any level of GM loss or gain in SUB (2.67 ± 0.92 vs. 1.92 ± 0.40 bursts/

min) or PHG inside versus outside the SOZ (2.24 ± 0.43 vs. 2.41 ± 0.58 bursts/min).

Discussion

Results from this study show that in patients compared to controls, there was a reduction in MTL GM thickness inside and outside the SOZ, yet there was a stronger association between GM loss and higher single neuron firing and burst rates inside than outside the SOZ. After adjusting for the effects of GM loss, analysis found significantly higher firing and bursting rates in several MTL subregions inside versus outside the SOZ at different levels of GM loss. These results suggest GM loss and correlation with firing rates is an important consideration for studies of epileptogenicity, and notably, provides evidence for interictal single neuron hyperexcitability in MTL structures capable of generating spontaneous seizures.

The reduction in MTL thickness inside and outside the SOZ observed in the group analysis is consistent with results from MRI studies that found ipsilateral, and in some studies contralateral, MTL atrophy in patients with temporal lobe (Jack et al., 1990; Cascino et al., 1991; Bernasconi et al., 1999, 2003) or extratemporal lobe epilepsy (Scott et al., 2003; Briellmann et al., 2004). Interpretation of the present structural data should consider that MRI parameters were optimized to enhance the structural detail in the MTL (Ekstrom et al., 2008), and subregion GM thickness was normalized to overall MTL size, not brain volume, which was not available with this protocol. It is unlikely the normalization methods would significantly affect outcomes because our analysis compared subject groups that were balanced for age and gender (Barnes et al., 2010), but it is possible that differences measured here might not be comparable beyond the MTL. In addition, we are aware that we may not know where seizures actually arose in some of our patients. If ictal onset occurred in areas where there were no electrode contacts, then apparent ictal onsets could reflect early propagation. MTL subregions without electrodes, but adjacent to sites of seizure onset, were included in the SOZ, as were subregions with early ictal propagation (Luders et al., 1993), which evidence suggests are areas inside the epileptogenic region (Lieb et al., 1986). In patients who underwent epilepsy surgery, resection included subregions identified inside the SOZ that was associated with seizure-free outcome.

In relation to MTL subregion, GM thickness in patients with respect to controls was significantly reduced in DG/CA2/CA3, SUB, EC, and FUS compared to CA1, PRC, or PHG. Subregions with GM loss were different compared to the classic pattern of hippocampal sclerosis (HS) in TLE, where greater neuron loss is found in the hilar region of DG, CA3, and CA1 than CA2 and portions of SUB (Mathern et al., 2008). Such differences should be expected, since only two patients in the current study had a diagnosis of HS, whereas the extent of subregion GM loss is consistent with the majority of patients who had MTL seizure onsets. Studies using similar segmentation techniques as the ones used here found in some patients with TLE and HS, diffuse GM loss in ipsilateral hippocampal formation, including evidence for contralateral damage in SUB (Hogan et al., 2004; Mueller et al., 2009). In addition, cases of TLE without MRI-detected HS, which were also included in the present study, had ipsilateral EC and SUB loss, whereas other cases had bilateral damage in DG and CA3 (Bernasconi et al., 2001; Mueller et al., 2009). Based on the different patterns of GM loss identified by MRI and histologic studies (Blümcke et al., 2007), it appears that there exist subtypes of HS, and imaging segmentation techniques like the ones used in the current study could help detect local MTL anatomic abnormalities. It is important to note, however, that in our study and others, MTL subregion margins were drawn manually rather than on the basis of distinct cytoarchitecture, which could not be detected on MRI. Higher resolution MRI and histologic studies are needed to determine how closely anatomic margins and subregion-specific GM loss corresponds with the different types of MTL pathology.

The observation that GM loss correlates with higher MTL firing and burst rates is consistent with the view that epileptogenicity in acquired epilepsy results from cell loss and synaptic reorganization of surviving neurons (Cavalheiro et al., 1982; Tauck & Nadler, 1985; Mathern et al., 1993). Furthermore, this correlation was stronger inside than outside the SOZ, which suggests that this mechanistic process is not obligatory, and reorganization in some areas appears to be much more epileptogenic than in others. By contrast, MTL GM loss outside the SOZ could be a secondary effect of recurrent epileptiform activity, although it is uncertain whether patient studies alone could distinguish between these two hypotheses. It is also not clear whether the correlation between GM loss and interictal neuronal hyperexcitability would be similar, for example, in an analysis consisting only of mesial temporal lobe epilepsy (MTLE). However, the significant morphologic alterations associated with HS often found in MTLE, combined with in vitro evidence demonstrating abnormal evoked responses correlate with severity of mossy fiber reorganizations (Masukawa et al., 1992), indicate that structure–function correlations could exist in MTLE and likely other epilepsies.

Several patient studies were unable to detect differences in interictal MTL firing rates in relation to the SOZ (Isokawa-Akesson et al., 1989; Viskontas et al., 2007; Le Van Quyen et al., 2008), whereas others, including our previous and current work, did find higher firing rates inside the SOZ (Isokawa-Akesson et al., 1987; Colder et al., 1996a; Staba et al., 2002a). The inconsistent results among patient studies could be due to differences in levels of antiseizure medication, although the recordings used here were carried out when patients were maintained at presurgical

levels that presumably should have reduced and made it more difficult to detect abnormal neuronal excitability. Rather, conflicting results could reflect sampling error when correlation with GM loss is not considered. Because hippocampal atrophy can be uneven (Ogren et al., 2009a,b), the present results indicate that measurement of GM loss as well as MTL subregion were important factors in detecting differences in firing and burst rates in relation to the SOZ, despite the relatively small number of patients; yet larger sample of single neurons compared to previous patient studies. In regard to MTL subregion, the largest differences in firing and bursts in relation to the SOZ were found in CA23DG, CA1, and EC, followed by SUB, and with no difference in PHG with GM loss. The regularity of abnormal firing across MTL subregions suggests localization of the microelectrode arrays on MRI was not associated with significant registration errors to obscure differences in firing with respect to subregion.

The functional significance of increased neuronal firing inside the SOZ is not yet known. It is possible that abnormal neuronal firing during interictal episodes strengthens synaptic connections through greater transmitter release and probability of synaptic transmission that maintains or increases the capacity of networks to generate spontaneous seizures (Bains et al., 1999). There is also evidence that networks capable of generating seizures have an enhanced ''sensitivity'' to depolarizing inputs (Jiruska et al., 2010). External impulses into these networks could drive hyperexcitable neurons that increase the synchrony of discharges, which was observed to be greater between single neurons inside versus outside the SOZ (Staba et al., 2002a,b). A combination of greater firing and synchrony could initiate a build-up of neuronal discharges that facilitates the transition from interictal to ictal (Babb & Crandall, 1976; Bower & Buckmaster, 2008; Cymerblit-Sabba & Schiller, 2010). Evaluation of these hypotheses should also consider cell type (e.g., principal and nonprincipal cells) and whether abnormal firing or bursting inside the SOZ is associated with excitatory or inhibitory cells, or both. Future investigations into the differences between the structure–function relationship of neurons in areas of GM loss inside and outside the SOZ should elucidate these aspects of synaptic reorganization that are epileptogenic.

Acknowledgments

This work was supported by the NIH/NINDS NS071048, NS002808, and NS033310. The authors thank Dr. Chuck Wilson for his review and valuable comments related to this work, and Eric Behnke and Tony Fields for their assistance with imaging and electrophysiologic data collection.

Disclosure

None of the authors has any conflict of interest to disclose. We confirm that we have read the Journal's position on issues involved in ethical publication and affirm that this report is consistent with those guidelines.

References

Amaral DG. (1999) Introduction: what is where in the medial temporal lobe. *Hippocampus* 9:1–6.

Babb TL, Crandall PH. (1976) Epileptogenesis of human limbic neurons in psychomotor epileptics. *Electroencephalogr Clin Neurophysiol* 40:225–243.

Bains JS, Longacher JM, Staley KJ. (1999) Reciprocal interactions between CA3 network activity and strength of recurrent collateral synapses. *Nat Neurosci* 2:720–726.

Barnes J, Ridgway GR, Bartlett J, Henley SM, Lehmann M, Hobbs N, Clarkson MJ, MacManus DG, Ourselin S, Fox NC. (2010) Head size, age and gender adjustment in MRI studies: a necessary nuisance? *NeuroImage* 53:1244–1255.

Bernasconi N, Bernasconi A, Andermann F, Dubeau F, Feindel W, Reutens DC. (1999) Entorhinal cortex in temporal lobe epilepsy: a quantitative MRI study. *Neurology* 52:1870–1876.

Bernasconi N, Bernasconi A, Caramanos Z, Dubeau F, Richardson J, Andermann F, Arnold DL. (2001) Entorhinal cortex atrophy in epilepsy patients exhibiting normal hippocampal volumes. *Neurology* 56:1335–1339.

Bernasconi N, Bernasconi A, Caramanos Z, Antel SB, Andermann F, Arnold DL. (2003) Mesial temporal damage in temporal lobe epilepsy: a volumetric MRI study of the hippocampus, amygdala and parahippocampal region. *Brain* 126:462–469.

Blümcke I, Pauli E, Clusmann H, Schramm J, Becker A, Elger C, Merschhemke M, Meencke H-J, Lehmann T, von Deimling A, Scheiwe C, Zentner J, Volk B, Romstöck J, Stefan H, Hildebrandt M. (2007) A new clinico-pathological classification system for mesial temporal sclerosis. *Acta Neuropathol* 113:235–244.

Bower MR, Buckmaster PS. (2008) Changes in granule cell firing rates precede locally recorded spontaneous seizures by minutes in an animal model of temporal lobe epilepsy. *J Neurophysiol* 99:2431–2442.

Briellmann RS, Jackson GD, Pell GS, Mitchell LA, Abbott DF. (2004) Structural abnormalities remote from the seizure focus: a study using T2 relaxometry at 3 T. *Neurology* 63:2303–2308.

Burggren AC, Zeineh MM, Ekstrom AD, Braskie MN, Thompson PM, Small GW, Bookheimer SY. (2008) Reduced cortical thickness in hippocampal subregions among cognitively normal apolipoprotein E e4 carriers. *NeuroImage* 41:1177–1183. PMC2601686.

Cascino GD, Jack CR Jr, Parisi JE, Sharbrough FW, Hirschorn KA, Meyer FB, Marsh WR, O'Brien PC. (1991) Magnetic resonance imaging-based volume studies in temporal lobe epilepsy: pathological correlations. *Ann Neurol* 30:31–36.

Cavalheiro EA, Riche DA, Le Gal La Salle G. (1982) Long-term effects of intrahippocampal kainic acid injection in rats: a method for inducing spontaneous recurrent seizures. *Electroencephalogr Clin Neurophysiol* 53:581–589.

Colder BW, Wilson CL, Frysinger RC, Harper RM, Engel J Jr. (1996a) Interspike intervals during interictal periods in human temporal lobe epilepsy. *Brain Res* 719:96–103.

Colder BW, Frysinger RC, Wilson CL, Harper RM, Engel J Jr. (1996b) Decreased neuronal burst discharge near site of seizure onset in epileptic human temporal lobes. *Epilepsia* 37:113–121.

Cymerblit-Sabba A, Schiller Y. (2010) Network dynamics during development of pharmacologically induced epileptic seizures in rats in vivo. *J Neurosci* 30:1619–1630.

Duvernoy HM. (1998) *The human hippocampus*. Springer, New York.

Ekstrom A, Suthana N, Behnke E, Salamon N, Bookheimer S, Fried I. (2008) High-resolution depth electrode localization and imaging in patients with pharmacologically intractable epilepsy. *J Neurosurg* 108:812–815.

Ekstrom A, Suthana N, Millett D, Fried I, Bookheimer S. (2009a) Correlation between BOLD fMRI and theta-band local field potentials in the human hippocampal area. *J Neurophysiol* 101:2668–2678.

Ekstrom AD, Bazih AJ, Suthana NA, Al-Hakim R, Ogura K, Zeineh M, Burggren AC, Bookheimer SY. (2009b) Advances in high-resolution imaging and computational unfolding of the human hippocampus. *NeuroImage* 47:42–49.

Engel J Jr. (1993) Outcome with respect to epileptic seizures. In Engel J Jr. (Ed.) *Surgical treatment of the epilepsies*. Raven Press, New York, p. 727.

Engel J Jr. (1996) Current concepts: surgery for seizures. *N Engl J Med* 334:647–652.

Engel SA, Glover GH, Wandell BA. (1997) Retinotopic organization in human visual cortex and the spatial precision of functional MRI. *Cereb Cortex* 7:181–192.

Fried I, Wilson CL, Maidment NT, Engel J Jr, Behnke E, Fields TA, MacDonald KA, Morrow JW, Ackerson L. (1999) Cerebral microdialysis combined with single-neuron and electroencephalographic recording in neurosurgical patients. Technical note. *J Neurosurg* 91:697–705.

Gourévitch B, Eggermont JJ. (2007) A nonparametric approach for detection of bursts in spike trains. *J Neurosci Methods* 160:349–358.

Gumprecht HK, Widenka DC, Lumenta CB. (1999) BrainLab VectorVision Neuronavigation System: technology and clinical experiences in 131 cases. *Neurosurgery* 44:97–104; discussion 104–105.

Hogan RE, Wang L, Bertrand ME, Willmore LJ, Bucholz RD, Nassif AS, Csernansky JG. (2004) MRI-based high-dimensional hippocampal mapping in mesial temporal lobe epilepsy. *Brain* 127:1731–1740.

Isokawa-Akesson M, Wilson CL, Babb TL. (1987) Structurally stable burst and synchronized firing in human amygdala neurons: Auto- and cross-correlation analyses in temporal lobe epilepsy. *Epilepsy Res* 1:17–34.

Isokawa-Akesson M, Wilson CL, Babb TL. (1989) Inhibition in synchronously firing human hippocampal neurons. *Epilepsy Res* 3:236–247.

Jack CR Jr, Sharbrough FW, Twomey CK, Cascino GD, Hirschorn KA, Marsh WR, Zinsmeister AR, Scheithauer B. (1990) Temporal lobe seizures: lateralization with MR volume measurements of the hippocampal formation. *Radiology* 175:423–429.

Jiruska P, Csicsvari J, Powell AD, Fox JE, Chang W-C, Vreugdenhil M, Li X, Palus M, Bujan AF, Dearden RW, Jefferys JGR. (2010) High-frequency network activity, global increase in neuronal activity, and synchrony expansion precede epileptic seizures in vitro. *J Neurosci* 30:5690–5701.

Labate A, Cerasa A, Gambardella A, Aguglia U, Quattrone A. (2008) Hippocampal and thalamic atrophy in mild temporal lobe epilepsy: a VBM study. *Neurology* 71:1094–1101.

Le Van Quyen M, Bragin A, Staba R, Crepon B, Wilson CL, Engel J Jr. (2008) Cell type-specific firing during ripple oscillations in the hippocampal formation of humans. *J Neurosci* 28:6104–6110. PMC2693199.

Lieb JP, Engel J Jr, Babb TL. (1986) Interhemispheric propagation time of human hippocampal seizures I. Relationship to surgical outcome. *Epilepsia* 27:286–293.

Lin JJ, Salamon N, Lee AD, Dutton RA, Gaeaga JA, Hayashi KH, Luders E, Toga AW, Engel J Jr, Thompson PM. (2007) Reduced neocortical thickness and complexity mapped in mesial temporal lobe epilepsy with hippocampal sclerosis. *Cereb Cortex* 17:2007–2018.

Luders HO, Engel J Jr, Munari C. (1993) General principles. In Engel J Jr (Ed.) *Surgical treatment of the epilepsies*. 2nd ed. Raven Press, New York, pp. 786.

Mai JK, Assheuer J, Paxinos G. (1997) *Atlas of the human brain*. Academic Press, San Diego, CA.

Masukawa LM, Uruno K, Sperling M, O'Connor MJ, Burdette LJ. (1992) The functional relationship between antidromically evoked field responses of the dentate gyrus and mossy fiber reorganization in temporal lobe epileptic patients. *Brain Res* 579:119–127.

Mathern GW, Cifuentes F, Leite JP, Pretorius JK, Babb TL. (1993) Hippocampal EEG excitability and chronic spontaneous seizures are associated with aberrant synaptic reorganization in the rat intrahippocampal kainate model. *Electroencephalogr Clin Neurophysiol* 87:326–339.

Mathern GW, Wilson CL, Beck H. (2008) Hippocampal sclerosis. In Engel J Jr, Pedley TA, Aicardi J, Dichter MA (Eds) *Epilepsy: a comprehensive textbook*. Lippincott Williams & Wilkins, Philadelphia, PA, pp. 121–136.

Matsumoto H, Marsan CA. (1964) Cortical cellular phenomena in experimental epilepsy: interictal manifestations. *Exp Neurol* 9:286–304.

McDonald CR, Hagler DJ, Ahmadi ME, Tecoma E, Iragui V, Gharapetian L, Dale AM, Halgren E. (2008) Regional neocortical thinning in mesial temporal lobe epilepsy. *Epilepsia* 49:794–803.

Mueller SG, Laxer KD, Barakos J, Cheong I, Garcia P, Weiner MW. (2009) Subfield atrophy pattern in temporal lobe epilepsy with and without mesial sclerosis detected by high-resolution MRI at 4 Tesla: preliminary results. *Epilepsia* 50:1474–1483.

Ogren JA, Wilson CL, Bragin A, Lin JJ, Salamon N, Dutton RA, Luders E, Fields TA, Fried I, Toga AW, Thompson PM, Engel J Jr, Staba RJ. (2009a) Three dimensional surface maps link local atrophy and fast ripples in human epileptic hippocampus. *Ann Neurol* 66:783–791.

Ogren JA, Bragin A, Wilson CL, Hoftman GD, Lin JJ, Dutton RA, Fields TA, Toga AW, Thompson PM, Engel J Jr, Staba RJ. (2009b) Three-dimensional hippocampal atrophy maps distinguish two common temporal lobe seizure-onset patterns. *Epilepsia* 50:1361–1370.

Reid SA, Sypert GW. (1980) Acute $FeCl_3$-induced epileptogenesis foci in cats: electrophysiological analyses. *Brain Res* 188:531–542.

Rutishauser U, Schuman EM, Mamelak AN. (2006) Online detection and sorting of extracellularly recorded action potentials in human medial temporal lobe recordings, in vivo. *J Neurosci Methods* 154:204–224.

Schlaier JR, Warnat J, Dorenbeck U, Proescholdt M, Schebesch KM, Brawanski A. (2004) Image fusion of MR images and real-time ultrasonography: evaluation of fusion accuracy combining two commercial instruments, a neuronavigation system and a ultrasound system. *Acta Neurochir (Wien)* 146:271–276; discussion 276–277.

Schwartzkroin PA, Turner DA, Knowles WD, Wyler AR. (1983) Studies of human and monkey "epileptic" neocortex in the in vitro slice preparation. *Ann Neurol* 13:249–257.

Scott RC, Cross JH, Gadian DG, Jackson GD, Neville BG, Connelly A. (2003) Abnormalities in hippocampi remote from the seizure focus: a T2 relaxometry study. *Brain* 126:1968–1974.

Selinger JV, Kulagina NV, O'Shaughnessy TJ, Ma W, Pancrazio JJ. (2007) Methods for characterizing interspike intervals and identifying bursts in neuronal activity. *J Neurosci Methods* 162:64–71.

Sherwin I. (1970) Burst activity of single units in the penicillin epileptogenic focus. *Electroencephalogr Clin Neurophysiol* 29:373–382.

Staba RJ, Wilson CL, Bragin A, Fried I, Engel J Jr. (2002a) Sleep states differentiate single neuron activity recorded from human epileptic hippocampus, entorhinal cortex and subiculum. *J Neurosci* 22:5694–5704.

Staba RJ, Wilson CL, Fried I, Engel J Jr. (2002b) Single neuron burst firing in the human hippocampus during sleep. *Hippocampus* 12:724–734.

Tauck DL, Nadler JV. (1985) Evidence of functional mossy fiber sprouting in hippocampal formation of kainic acid-treated rats. *J Neurosci* 5:1016–1022.

Teo PC, Sapiro G, Wandell BA. (1997) Creating connected representations of cortical gray matter for functional MRI visualization. *IEEE Trans Med Imaging* 16:852–863.

Viskontas IV, Ekstrom AD, Wilson CL, Fried I. (2007) Characterizing interneuron and pyramidal cells in the human medial temporal lobe in vivo using extracellular recordings. *Hippocampus* 17:49–57.

Wilbur WJ, Rinzel J. (1983) A theoretical basis for large coefficient of variation and bimodality in neuronal interspike interval distributions. *J Theor Biol* 105:345–368.

Zeineh MM, Engel SA, Thompson PM, Bookheimer SY. (2001) Unfolding the human hippocampus with high resolution structural and functional MRI. *Anat Rec* 265:111–120.

Zeineh MM, Engel SA, Thompson PM, Bookheimer SY. (2003) Dynamics of the hippocampus during encoding and retrieval of face-name pairs. *Science* 299:577–580.

Supporting Information

Additional Supporting Information may be found in the online version of this article:

Figure S1. Wide bandwidth microelectrode recordings, action potential detection, and cluster analysis.

Table S1. Unadjusted mean firing rates in relation to SOZ and MTL subregion by patient.

Please note: Wiley-Blackwell is not responsible for the content or functionality of any supporting information supplied by the authors. Any queries (other than missing material) should be directed to the corresponding author for the article.